PCCP

PAPER

Cite this: *Phys. Chem. Chem. Phys.*, 2017, **19**, 23397

Critical adsorption of periodic and random polyampholytes onto charged surfaces†

Daniel L. Z. Caetano,[a] Sidney J. de Carvalho,[a] Ralf Metzler[b] and Andrey G. Cherstvy*[b]

Received 15th June 2017,
Accepted 8th August 2017

DOI: 10.1039/c7cp04040g

rsc.li/pccp

How different are the properties of critical adsorption of polyampholytes and polyelectrolytes onto charged surfaces? How important are the details of polyampholyte charge distribution on the onset of critical adsorption transition? What are the scaling relations governing the dependence of critical surface charge density on salt concentration in the surrounding solution? Here, we employ Metropolis Monte Carlo simulations and uncover the scaling relations for critical adsorption for quenched periodic and random charge distributions along the polyampholyte chains. We also evaluate and discuss the dependence of the adsorbed layer width on solution salinity and details of the charge distribution. We contrast our findings to the known results for polyelectrolyte adsorption onto oppositely charged surfaces, in particular, their dependence on electrolyte concentration.

I. Introduction

Polyampholyte (PA) chains are hetero-polymers consisting of positive, negative, and neutral monomers.[1–9] Various physical–chemical properties of PAs find a broad range of applications[6,10] in *e.g.* paper production processes, water desalination, colloid stabilisation and flocculation, wetting and lubrication, and adhesion, as well as other modifications of surface properties. The PAs are also used as synthetic vectors for gene delivery applications[6,11] and as model systems to study charge-stabilised polypeptides and intrinsically disordered proteins.[12,13]

The phase behaviour, solubility, viscosity, conformational and hydrodynamic properties of PAs have been systematically studied (see ref. 1 and 6 for an overview). The charged state of the PA sites can depend on the pH value, resulting in "annealed" rather than "quenched" charge distributions. The effects of the net charge on the configurations and shape of PAs have been studied theoretically and experimentally.[1,4,14–19] In particular, elongation, coil-to-globule transition, and necklace formation for PA chains have been examined.[1,6] The variation of the pH value and charge asymmetry is known *e.g.* to affect the position of the globule-to-coil transition for PAs.[6]

The properties of PAs near charged interfaces are of biological relevance, *i.a.* for the behaviour of polypeptides near charged constituents in biological cells (*e.g.* near negatively charged lipid membranes[20–22]). The polypeptide chains are composed of different amino-acid residues with widely varying physical–chemical, hydrophilic, and surface-adsorption properties. Protein dynamics, protein folding in solutions,[23] and protein unfolding *via* attractive surfaces[24] possess some similarities with the behaviour of PAs near charged surfaces.

Similar to adsorption of polyelectrolytes (PEs),[7,25–35] the adsorption of PAs onto charged surfaces as well as onto nanoparticles[36] (polystyrene latex, mica, silica, *etc.*) has been examined experimentally[37–42] and theoretically (see ref. 4 and 43–45 and the discussion below). The experimental techniques used to measure the thickness of the adsorbed polymer layer include ellipsometric, spectroscopic, potentiometric, plasmon resonance, hydrodynamic, and electrophoretic mobility measurements. The adsorption of net-charged PAs onto similarly charged surfaces is possible (wrong side of the isoelectric point), as observed *e.g.* for the negatively charged gelatin chains.[1,36,41,42,46] As possible applications, we mention also the interactions of charged polymers (such as DNA, RNA, *etc.*) with the pore walls and membranes in polymer translocation experiments[47] as well as the formation of DNA knots and denaturation bubbles[48,49] induced by surface adsorption.

The adsorption transition of PAs in front of charged surfaces takes place as a consequence of chain polarisation in the electric field.[4,43,44] PA adsorption onto planar and curved surfaces has been the subject of intense research,[3,4,50–52] with random charge distributions along PAs being often considered.[4] Important trends in PA–surface adsorption were uncovered,[43,53–59] including the behaviour of weak titratable chains,[60] diblock[61,62] and multiblock PAs,[63,64] PA chains inside slit geometries, complexes of

[a] *Sao Paulo State University (UNESP), Institute of Biosciences, Humanities and Exact Sciences (Ibilce), Campus Sao Jose do Rio Preto, 15054-000, Brazil. E-mail: daniel.caetano@sjrp.unesp.br, sidneyjc@ibilce.unesp.br*

[b] *Institute for Physics & Astronomy, University of Potsdam, 14476 Potsdam-Golm, Germany. E-mail: rmetzler@uni-potsdam.de, a.cherstvy@gmail.com*

† Electronic supplementary information (ESI) available. See DOI: 10.1039/c7cp04040g

PAs with nanoparticles[65,66] and PEs.[1] Specifically, the adsorption of PAs onto charged surfaces in the three basic geometries—planar, cylindrical, and spherical—was considered.[51] The effect of block length on the distributions of periodic PAs near the adsorbing plane in the absence of screening was examined by simulations.[63]

Recently, the conformations of PAs near a uniformly charged rod and salt-induced transitions have been considered.[64] It was demonstrated that at higher salt concentrations a transition occurs from large-loop PA conformations to "necklace"-like PA complexes parallel to the cylinder.[64] The properties of both single- and multi-chain[44] PA adsorption onto surfaces were studied, both theoretically and by computer simulations. The effects of solvent quality and dielectric permittivity value on PA–surface adsorption were also rationalised.[53] Note, however, that often a non-screened version of the electrostatic (ES) potential is implemented in simulations.[50,63]

One vivid difference of PA– *versus* PE–surface adsorption is that—due to non-uniform distributions of non-identical monomers along the PA chains—their adsorption onto charged interfaces can produce some "star-like" structures, as well as "trains" and "arms" of irregular length,[30] emerging as a response to a particular PA charge pattern (see Fig. 1). We refer also to a recent study[64] for a detailed overview of PA-rod adsorption.

The adsorption–desorption ES-driven first-order phase transition of PEs and PAs onto charged surfaces is a critical phenomenon.[35,67] In equilibrium, at the threshold curve the ES attractive interactions of the polymer to the interface are exactly balanced by the entropy losses accompanying chain confinement near the surface. For PE chains, the general adsorption trends and critical adsorption conditions onto oppositely charged surfaces were studied for planar[34,35,67–77] and curved[34,71,77–90] interfaces, as well as in confinement.[91–93] The scaling behaviour of critical surface charge density, σ_c, required for PE adsorption onto the weakly charged plane is[7,34,67,69,75,79]

$$\sigma_{c,PE}(\kappa) \sim \kappa^3, \quad (1)$$

where $\kappa = 1/\lambda_D$ is the reciprocal Debye screening length in the solution. Physically, as more salt is added to the solution, the PE–surface ES attraction is screened better and thus larger surface charge densities are required to ensure polymer adsorption. The values of σ_c for critical PE-plane adsorption get reduced at lower temperatures T, higher PE linear charge densities ρ, and shorter polymer persistence lengths l_p, composing the universal adsorption parameter yielding $|\sigma_{c,PE}| \sim \varepsilon k_B T l_p \kappa^3/|\rho|$ (see ref. 35). This expression provides the critical adsorption characteristic in terms of physical–chemical parameters potentially controlled in experiments. The adsorption of periodic PEs with block-like charge structures onto charge-patterned surfaces was also studied,[72,94] as a function of patch size and surface and polymer charge densities (see also ref. 95 for general ES of patchy surfaces).

The properties of *critical* adsorption of PAs onto charged interfaces have not been examined, however, to the best of our knowledge. The PA–surface adsorption is known to be driven by polarisation effects and short-ranged non-ES contacts.[6,54,57,96] A multitude of PA conformations in solution—as compared to *e.g.* a swollen state of a weakly charged PE chain in the absence of condensed counterions[97,102,104,105]—together with often irregular PA charge distributions, makes the general problem of critical PA–surface adsorption interesting and challenging, both analytically and by simulations. This is the main subject of the current study.

In particular, we study the effects of varying Debye screening length λ_D in tuning the strength of ES chain–surface contacts. Similarly to PE adsorption, the adsorption–desorption transition of PAs is expected to take place when the entropic free energy of the chain in the desorbed/free state overcomes the energy of its ES binding to the interface in the adsorbed state, with the energetic barrier of the order of thermal energy, k_BT.[44] We unravel the adsorption–desorption curve $\sigma_c(\kappa)$ *via* extensive simulations, quantifying the statistics of polymer–surface contacts under conditions close to thermodynamic equilibrium. The current study thus adds an important bit of information to the—often quite approximate—scaling relations derived theoretically for PA–surface adsorption.

The paper is organised as follows. In Section 2, we discuss the approximations and present the details of our computer simulations. We consider the ES interactions within the chain and with the adsorbing interface; the effects of fine parameters of PA charge distributions are examined too. In Sections 3 and 4 we overview the main findings on monomer distributions and critical adsorption conditions of PA chains onto negatively charged planes. We examine the adsorption conditions of a single PA chain onto surfaces with varying charge density σ.

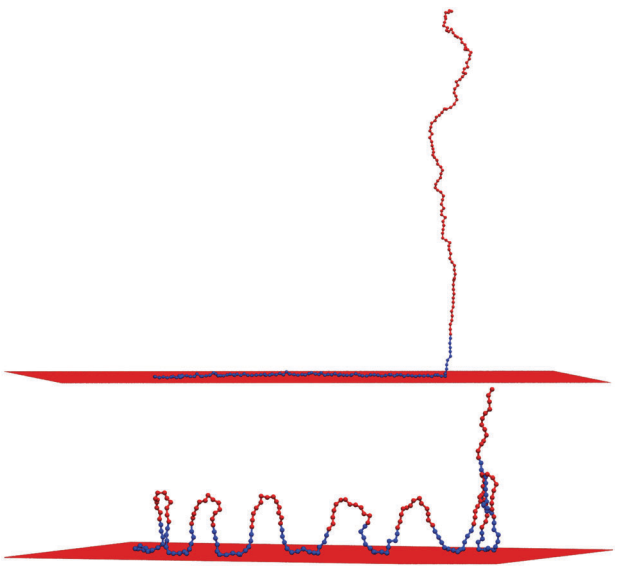

Fig. 1 Snapshots of typical configurations of periodic PAs near negatively charged surfaces, as obtained from simulations. Parameters: the surface charge density is $\sigma = -0.1$ C m^{-2}, the salt concentration is $n_0 = 10^{-3}$ M, and the chain polymerisation degree is $N = 208$. The top and bottom panels show the PAs with two and sixteen blocks, so that the block length is $n = 104$ and 13, respectively. Negative monomers are red beads, positive monomers are blue beads. Video files illustrating PA adsorption dynamics to the surface in the electrolyte solutions with salt concentrations $n_0 = 10^{-3}$ M ($\lambda_D \approx 96$ Å), 0.1 M ($\lambda_D \approx 9.6$ Å), and 0.25 M ($\lambda_D \approx 6.1$ Å), recorded during 10^4 simulation steps for diblock and hexadecablock PA chains, are included in the ESI.†

In Sections 3 and 4, we examine the behavior of PA chains with periodic[106] and random charge distributions, respectively. Finally, in Section 5, we outline possible applications of our results and extensions of the model.

II. Model, approximations, and simulation methods

We employ the standard linear Poisson–Boltzmann equation[34,35] to compute the ES potential $\phi_{ES}(x)$ emerging from the planar uniformly-charged interface. This external potential defines the magnitude of ES interactions of all N PA monomers with the surface, namely

$$E_{ES}^{ext} = -\sum_{i=1}^{N} \pm e_0 \phi_{ES}(x_i) = \sum_{i=1}^{N} \pm e_0 \frac{4\pi|\sigma|}{\varepsilon\kappa} e^{-\kappa x_i}, \qquad (2)$$

where x_i is the distance of the ith monomer from the flat surface. For a negatively charged surface, the "plus" sign above is taken for negative PA monomers (that is, for unfavourable ES energy), whereas for positive PA charges the ES interaction energy in eqn (2) is negative (the "minus" sign above, as PA–surface contacts are beneficial). The potential distributions $\phi_{ES}(r)$ in simple 1:1 electrolyte—*i.e.* monovalent cations and anions—near charged surfaces of different geometries were summarised in ref. 34, 35, 77 and 92. The physical limits of applicability of the linear Poisson–Boltzmann solution (2) were discussed in our recent study,[77] where the properties of PE–surface adsorption for linear and nonlinear ES potentials were examined. We showed *e.g.* that for a charged plane the critical surface charge densities σ_c for the linear and nonlinear theories are very close as soon as $\kappa \lesssim 0.2$ Å^{-1}.

We also assume below that the dielectric constant attains its bulk value even close to the highly charged surfaces, $\varepsilon(x) = \varepsilon$, and also in the PA vicinity. In reality, the ES-induced ordering of water molecules near significantly charged interfaces makes the dielectric response anisotropic, with often a much lower effective permittivity near the surface. Also note that the adsorption of PA chains in experiments often takes place onto non-polar media, such as silica surfaces and latex particles, with dielectric permittivities $\varepsilon_c \ll \varepsilon$. The additional ES repulsion of image charges induced underneath the interface[4] "displaces" the charged polymer from the attracting surface and therefore larger surface charge densities are required to achieve adsorption onto a low-dielectric substrate. The detailed analytical consideration of the image-charge effects for critical PE–surface adsorption was presented in ref. 80, including changes in scaling of σ_c *versus* κ. The effects of image charges are particularly pronounced at low salt concentrations, as expected. A systematic investigation of the ε_c-effects on PA–surface adsorption is, however, beyond the scope of the current study.

The ES interactions of PA monomers within the chain are the sum of exponentially screened (internal) Coulomb contributions at inter-charge distances r_{ij}, namely

$$E_{ES}^{int} = \sum_{i,j,i\neq j} \pm e_0^2 e^{-\kappa r_{ij}} / (\varepsilon r_{ij}). \qquad (3)$$

Here

$$\kappa = \sqrt{8\pi l_B n_0} = \lambda_D^{-1} \qquad (4)$$

is the inverse Debye length at salt concentration n_0,

$$l_B = e_0^2/(\varepsilon k_B T) \approx 7.1 \text{ Å} \qquad (5)$$

is the Bjerrum length, $\varepsilon = 78.7$ is the dielectric constant of the solution, and $T = 298.15$ K is the absolute temperature. In our simulations two consecutive monomers are connected by the harmonic potential, so that the total Hookean elastic energy is

$$E_{el} = \sum_{j=1}^{N-1} k(b_j - b_0)^2 / 2, \qquad (6)$$

where $k = 1.0$ N m^{-1} and $b_0 = 7.0$ Å is the average distance between the neighbouring PA beads carrying the elementary charge $+e_0$ or $-e_0$ (see also Fig. 3). The chain contains no neutral monomers. The additional hard-core potential is added to (3) in order to avoid the overlap of PA beads.[64] The Debye–Hückel repulsion of PA charges of the same sign gives a positive contribution in eqn (3), whereas the ES energy is negative for the attraction of oppositely charged PA beads. Non-ES or specific chemical interactions—that can affect the polymer adsorption behaviour[96]—are not taken into account, for simplicity (see the Discussion section for some details).

We are interested in the PA adsorption characteristics in the single-polymer limit, often under conditions close to the adsorption–desorption coexistence line. In this situation, one can neglect the effects of mutual interactions between the fragments of the adsorbed chain. We use the same simulation procedure as implemented recently for simulating critical PE–surface adsorption.[77,79,89,90,91] The inter-monomer ES and non-ES potentials and the simulation methods are the same as for (above-critical) PA–cylinder adsorption in ref. 64. This reference contains a detailed analysis of PA conformations and physical principles of polymer adsorption. We perform Metropolis Monte Carlo simulations in the canonical *NVT* ensemble. The equilibration is reached after $\sim 10^7$ steps and we account for $\sim 10^7$ statistically independent configurations of the chain—the same as the number of simulation steps—to calculate average quantities and monomer distributions.

We observe that—for a given surface charge density σ and salt concentration n_0 not far away from the critical transition line—the polymer undergoes transitions between the coexisting adsorbed and desorbed states (see Fig. 1 and video files in ESI†). Varying the surface charge density in simulations, the critical σ_c value is found according to the procedure similar to that used in our previous works.[77,79] The adsorbed state is characterised by the ES binding energies of up to several k_BT per monomer (see Fig. 5 and 9). In contrast, in the desorbed state the PA chain has a rather weak binding energy (often close to zero). With increasing salt concentration or decreasing surface charge density, the fraction of PA configurations in the desorbed state increases due to weaker ES attraction to the surface. The difference of PA binding energies in the adsorbed and desorbed states allows us to compute the overall fraction of PA

configurations in each state, in the course of simulations. We define the critical surface charge density $\sigma = \sigma_c$ such that the number of configurations in the adsorbed and desorbed states is equal, the ''50/50'' rule.

Note that several other polymer adsorption criteria exist in the theoretical and simulational literature. Some of them, *e.g.*, involve a criterion for confinement of most of the polymer monomers within a thin—but not universal as a function of the system parameters—layer near the interface. The issue is similar to that for defining the condensed *versus* free counterions in the double layer near highly charged interfaces. The ''50/50'' criterion on chain configurations we use allows, however, a better sampling of polymer coexistence in the adsorbed and desorbed states, as compared to other adsorption criteria employing thin-layer shells or binding-energy thresholds. Therefore, at σ_c the number of PA configurations in both the adsorbed and desorbed states is the same.[77,79,91,120] Note, however, that for ''inverse'' PE–surface adsorption in confinement,[91] we often did not observe the adsorption–desorption transition and the value of σ_c was defined as the surface charge density at which the PE–surface binding energy $|E_{ES}^{ext}| \gtrsim k_B T$. The monomer radius in simulations below is $R = 2$ Å and the charges are positioned in the centre of each bead.[79,91] The reader is referred to ref. 77 for the effects of the monomer size on PE–surface adsorption.

For net-neutral PAs—the only situation considered below—the number of positive N_+ and negative N_- charges is identical, so that the charge asymmetry parameter,[4]

$$f = (N_+ - N_-)/(N_+ + N_-), \quad (7)$$

is zero. When positive charges prevail in the PA chain, the parameter f attains positive values, $0 < f < 1$. For net-neutral random PAs, the fluctuation-induced attractions between the charges keep short chains close to the Gaussian coil state, whereas at length-scales larger than the typical blob size the chain becomes more compacted. For a progressive accumulation of non-compensated charges, the chains of random PAs adopt ES-stretched cylinder-like conformations and, finally, ''necklace''-like structures.[4] The latter emerge due to the competition of the fluctuation-induced ES attraction of neighbouring monomers[104,107] and (screened) Coulomb repulsion of excess PA charges.[4] One expects that—as the charge asymmetry grows, $f > 0$, and more positive monomers are brought in contact with the negative interface—the critical charge density $|\sigma_c|$ for PA adsorption should decrease. In contrast, for negative charges prevailing in the chain, $f < 0$, higher $|\sigma_c|$ values are expected. The detailed analysis of critical adsorption conditions for PAs with non-zero net charges is, however, the subject of a separate study.

For net-neutral PA chains, a random positioning of charges along the polymer can be mimicked by a random walk, with its direction of motion on each step defining the sign of the charge on a given monomer.[1] For periodic PAs, the charge distribution is a simple alternating sequence of n positive and n negative charges. By construction, the entire PA is then neutral. To define the charge distribution for random PAs—in order to start the simulations—we first attribute positive or negative monomers randomly along the chain, with equal probability at each bead. If the polymer is not neutral after this, we chose randomly a monomer with the same charge sign as that of the whole chain, and revert its charge. This procedure is repeated until we obtain a neutral PA chain that possesses a random positive–negative charge distribution (no neutral monomers). The results in Section 4 are obtained after averaging over multiple different initial PA random-charge configurations.

III. Periodic PA charge distributions

In this section, we present the results of simulations for monomer distribution profiles, bond length distribution, width of the adsorbed layer, and conditions of critical adsorption for PAs with periodic patterns of positive and negative charges onto a negatively charged planar surface.

A. Monomer density profiles $\rho_{\pm}(x)$

Above the adsorption threshold—for highly charged surfaces $\sigma > |\sigma_c|$ and low concentrations of simple salt in the solution $\kappa < \kappa_c$[34,35]—the PA chains form an adsorbed layer on the surface (see Fig. 2). Its width or thickness is determined as the distance from the interface containing half of the PA monomers, of both positive and negative charge, during the simulation time. To compute the net cumulative PA charge per surface area, we can integrate the monomer density distribution, $e_0[\rho_+(x) - \rho_-(x)]$, from the interface at $x = 0$ up to position x.

We find that periodic PAs with $f = 0$ can adsorb onto a sufficiently charged plane if the patches of charges of the same sign along the chain are long enough. The PA chains are confined near the interface so that the adsorbed ''trains'' of positive charges are attracted by ES forces to the negative surface and the desorbed loops of negative charges repelled from the surface alternate along the contour (see Fig. 5 below and the video files in the ESI;† compare also to some experimentally proposed conformations[42]). The length of surface-adsorbed segments is correlated with the length of positively charged PA blocks, $l = nb$, particularly at low salt concentrations. Such quasi-regular structures are similar to the ''rosette'' states for PE adsorption[103] and also ''star-like'' structures for PA adsorption[43] onto charged spherical particles. At a given surface charge density σ, the PAs with shorter charge patches adsorb as progressively more extended layers near the surface (see Fig. 2 and below).

The video files in the ESI† visualise the dynamics of the diblock and hexadecablock PA chains adsorbed to the surface. The mid-point PA monomer is positioned at the centre of the visible surface in the videos, so that the rotational dynamics and binding–unbinding events can be observed. The positive block of the diblock chains at relatively low salt concentration ($n_0 = 10^{-5}$ M) is strongly bound, whereas the negatively charged block is strongly repelled from the surface, as expected. This causes the maximal stretching of the polymer at its central monomer, where the blocks are connected. We find that PA conformations for almost unscreened ES interactions are very regular, for both diblock and multiblock PAs.

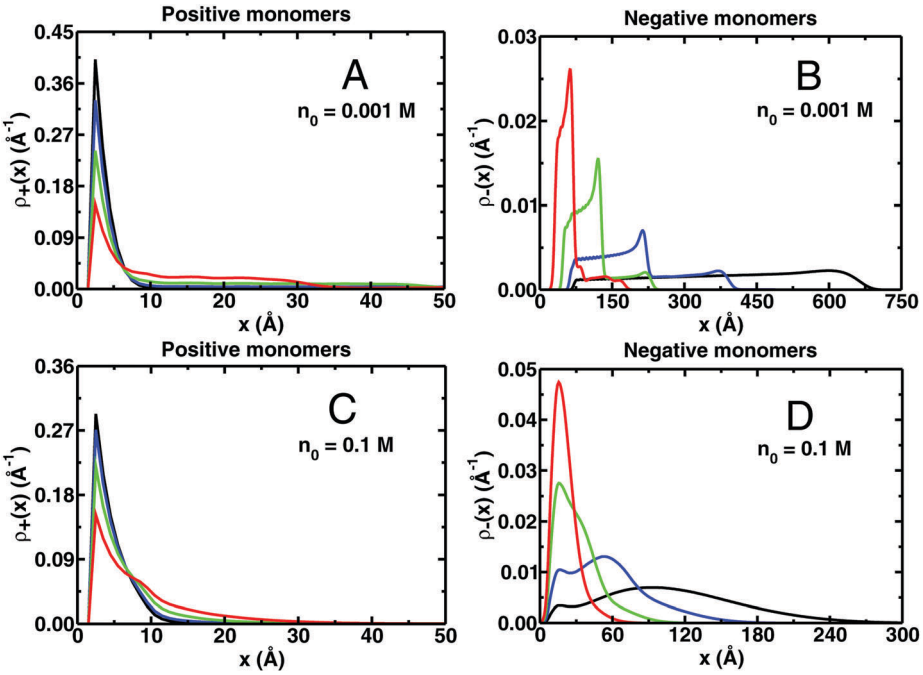

Fig. 2 Density distributions of positive $\rho_+(x)$ and negative $\rho_-(x)$ monomers of a PA chain near the negatively charged flat surface, at the surface charge density above the adsorption transition. Parameters: the salt concentration is, respectively, n_0 = 0.001 M and 0.1 M for the top and bottom panels, the surface charge density is $\sigma = -0.1$ C m^{-2}, the PA charge asymmetry is f = 0, and the chain length is N = 208. The PA charge periodicity of n = 13 (red), 26 (green), 52 (blue), and 104 (black curves) monomers corresponds to hexadecablock, octablock, tetrablock, and diblock chains, respectively.

At very low salt, the hexadecablock PAs are in the ''train'' and ''loop'' states. For diblock PAs, large changes in the adsorption dynamics occur between n_0 = 100 mM and 250 mM of simple salt, whereas for hexadecablock PA chains more pronounced changes are observed to take place between 1 mM and 100 mM of salt in the solution. At higher salt amounts the adsorbed chains acquire progressively more freedom: the number of adsorbed PA conformations increases and switching between them takes place constantly in the simulations. The PA chains at large salt amounts are only weakly bound to the surface and much more intermingled/knotted[114] and irregular in shape. These internal inter-connections and links strongly affect the chain dynamics, whereas the ES forces—both of attractive and repulsive nature—are strongly screened in the limit of high salt. Note that the statistics of PA chains perpendicular to the ES gradient remains unchanged (along the interface), whereas it is strongly non-Gaussian in the direction perpendicular to the interface, particularly in strong adsorption regimes (low n_0 and high $|\sigma|$ values).

Fig. 2 illustrates the density profile $\rho_\pm(x)$ of monomers of adsorbed periodic PAs. We observe that positive PA monomers are ES-attracted to the negatively charged surface, being close to the interface. In contrast, negative PA monomers are repelled from the interface to a large distance, compare the left and right columns of Fig. 2 for $\rho_+(x)$ and $\rho_-(x)$. At lower solution salinities—when both the attractive and repulsive ES interactions get amplified—the distributions of positive PA monomers $\rho_+(x)$ get closer to the surface, whereas the profile of negative PA monomers $\rho_-(x)$ gets substantially more extended into the solution. The results for different salt concentrations are shown in the top and bottom panels of Fig. 2. For longer PA chains, the distribution $\rho_-(x)$ becomes even more expelled from the surface, whereas the profiles of ES-attracted positive monomers on longer PAs appear closer to the interface (results not shown).

The effect of periodicity n of patches of the same charge along PAs is as follows. For shorter block lengths the positive monomers show a profile more extended from the interface; compare the red and black curves for $\rho_+(x)$ in Fig. 2. For negative PA monomers, we find that at large separations from the interface there is a significant peak in the $\rho_-(x)$ distribution, particularly pronounced for the conditions of low salinities and long charge blockiness n. This is due to ES repulsion of longer PA stretches of the same charge from the surface. Overall, negative PA monomers displaced away from the interface by ES repulsions are much further from the boundary, as expected intuitively; compare the panels $\rho_\pm(x)$ in Fig. 2.

Also, as the salt concentration increases in Fig. 2 from n_0 = 0.001 M to 0.1 M, the negative PA monomers get distributed in a closer proximity to the interface. The ES repulsions of negative PA monomers from the negative surface get diminished at higher salt and negative patches thus more readily follow the blocks of ES-attracted positive PA charges.

Note that the distribution of PA bond lengths is rather broad but it gets only slightly altered upon such a change in the solution salinity, Fig. 3. As the average monomer–monomer distance is $b_0 \approx 7$ Å and the monomer radius is 2 Å, the free space between the two neighbouring monomer surfaces is $\approx$3 Å. Thus, on average, the hard-core potential in our model

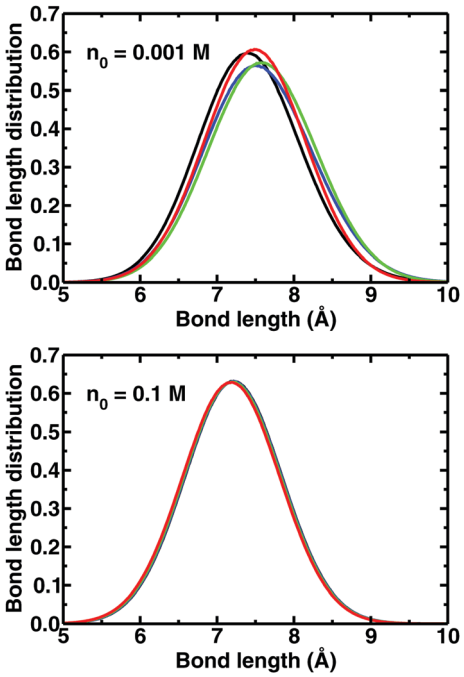

Fig. 3 Distribution of PA bond lengths for the salt concentration of n_0 = 0.001 M and 0.1 M, computed for $\sigma = -0.1$ C m^{-2}. The colour scheme is the same as in Fig. 2.

prevents bonds between the monomers from slipping over each other. We also checked that the equilibration of the bond length is achieved (for tetrablock PA chains) under these conditions after $\sim 5 \times 10^6$ simulation steps.

B. Adsorbed layer width w

Above the adsorption–desorption transition,[34,35] the width of adsorbed layers w is an important experimental characteristic for both PE– and PA–surface adsorption.[7,28,35,70] Theoretically, the layer width of adsorbed random PAs was predicted[4,44] to change only slightly if the Debye length λ_D is shorter than the Gouy–Chapman length,[108]

$$\lambda_{GC} = e_0/(2\pi l_B|\sigma|), \quad (8)$$

(see also Section 4). With increasing salt concentrations n_0—when the adsorbed layer width w becomes comparable to λ_D—the PA layer width w_{PA} starts to decrease.[4,44] This trend is opposite to that for PE adsorption on oppositely charged surfaces, where the relation

$$w_{PE}(\sigma) \sim \sigma^{-1/3} \quad (9)$$

was theoretically predicted in the dilute regime (single-chain limit).[7,25,34,35,74,75,109,110] We discuss this relation below for different definitions of the PA layer width. For experiments probing relation (9) the reader is referred to the original studies listed in ref. 7, 74 and 75. The width of adsorbed PE layers is also known to increase with salt concentration,[35] in agreement with experimental evidence.[111] Theoretically, for the conditions above the adsorption threshold, smaller $|\sigma|$ and larger κ values "drive" the system towards the adsorption transition curve, where the adsorbed layer width diverges.[34,35]

The Monte Carlo simulations of ref. 50 showed that the thickness of the adsorbed PA layers near a non-screened charged plane ($n_0 = 0$) is non-monotonic with σ. The layer width w first increases, then saturates, and finally it starts to decrease as $|\sigma|$ increases. We here detect similar trends (see Fig. 4 and the discussion below). Also note that, due to a finite PA monomer volume in reality, the scaling theoretical predictions for the layer thickness[4] *versus* the chain length N for infinitely thin chains need to be modified.[50] We quantify the adsorbed layer width for PA–surface adsorption at varying interface charge density in Fig. 4. In this figure, we use $n_0 = 10^{-5}$ M, to be closer to a salt-free system and plot the results up to the charge density of -0.1 C m^{-2}. Note that at even larger $|\sigma|$ and lower salinities the links connecting PA beads acquire a considerable stretching.

We use several methods and measures to quantify the PA layer width, namely w_h, w_h^{pos}, w_{50}, and R_g^x. The layer width on 1/2 of the height of the peak in the distribution of all PA monomers, $\rho_+(x) + \rho_-(x)$, is denoted as w_h. The same computed from the density distribution of only positive monomers in the adsorbed peak is denoted as w_h^{pos}. The layer width encompassing about 50% of all the PA monomers independent of their charge is w_{50}. Finally, the layer width can be characterised by the chain's radius of gyration in the direction normal to the interface, R_g^x. For PA–cylinder adsorption, the component analysis of the gyration tensor was performed recently.[64]

Depending on a given physical problem, one or another width quantifier can be preferred. The layer width based on half-height of the surface-adsorbed monomer profile gives us a "local" description of bound monomers. This method works best for well-defined short-tail monomer profiles. In the limit of large $|\sigma|$ it produces the same scaling (9) for both PE– and PA–surface adsorption. In contrast, the radius of gyration is a global measure of polymer dimensions, assessing better the overall extension. For instance, this is the case for PA profiles extended substantially normal to the interface and lacking a pronounced first-adsorption peak; see some representative PA configurations at small $|\sigma|$ presented in Fig. 5.

We start with the results for $w_h(\sigma)$ and $w_h^{pos}(\sigma)$. Consistent with the monomer density distributions in Fig. 2, we find that for weakly charged surfaces the PA chains with shorter block length reveal a larger layer width w_h (see Fig. 2A and 4A). For highly charged surfaces the layer width is almost independent of charge periodicity n and in this regime universal scaling (9)—similar to that for PE–surface adsorption—is observed. The longer the charge block length n, the smaller the surface charge density $|\sigma|$ after which this large-σ scaling becomes valid, as expected; compare the red, green, blue, and black curves in Fig. 4A for n = 13, 26, 52, and 104 monomers, respectively.

For the layer width from the distribution of only positive monomers, we find rather similar trends. Also, in the limit of large $|\sigma|$ we recover for $w_h^{pos}(\sigma)$ dependence the same PE-related scaling (9) (Fig. 4B). At smaller $|\sigma|$, however, only the PA chains with the longest charge periodicity are strongly adsorbed and follow eqn (9). In this regime, we observe that the PA layer is

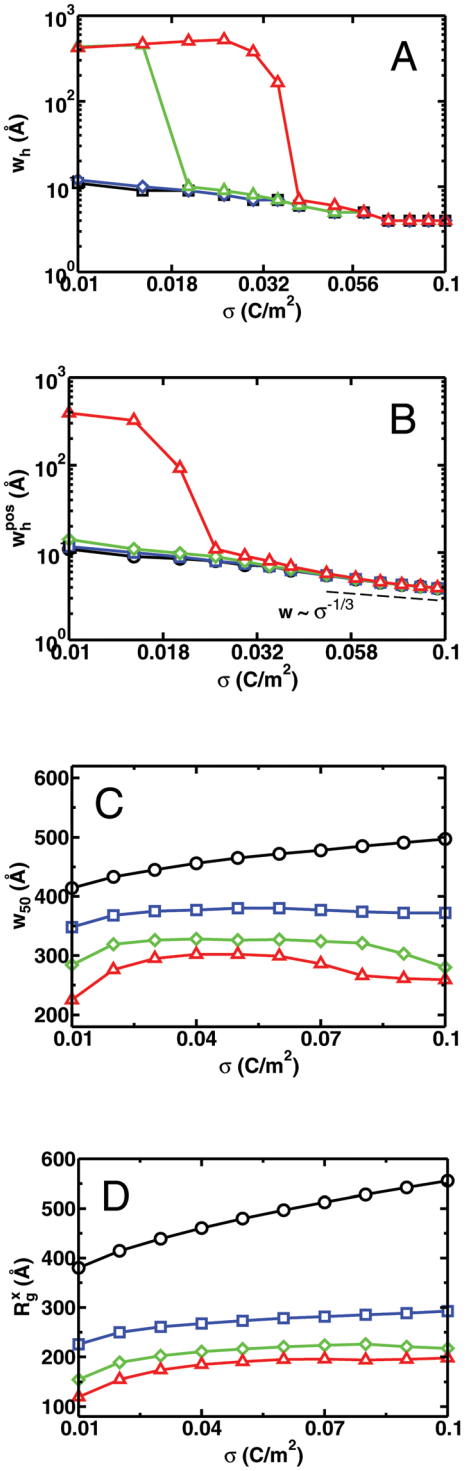

Fig. 4 Width of surface-adsorbed layers of PAs with periodic charge distributions *versus* the surface charge density $|\sigma|$. Panels (A and B) show the width at 1/2 of the height, computed from the distributions of all the PA monomers and from $\rho_+(x)$ only (see the text). The asymptote of eqn (9) is the dashed line in the large-σ limit. Panel (C) shows the layer width where 50% of all the PA monomers are located. Panel (D) is the chain's gyration radius normal to the interface. The colours are the same as in Fig. 2: n = 13 (red), 26 (green), 52 (blue), and 104 (black symbols). The simulation time to produce a point of this plot for a given charge density on a standard single-core workstation is ~3 days. Parameters: $n_0 = 10^{-5}$ M (corresponding to $\lambda_D \approx 960$ Å), f = 0, and N = 208.

much thinner than the Debye screening length λ_D. The PA chains with shorter periodicities—n = 13 and n = 26 in Fig. 4A and B—reveal very large widths w_h and w_h^{pos} for small surface charge densities.

At a particular surface charge density the layer width characterised by these two quantifiers rapidly drops from very large values towards the asymptote described by eqn (9). We verified that large values of w_h and w_h^{pos} at small $|\sigma|$ occur because the chain is mostly normal to the surface, and thus the first peak of the monomer distribution profile is small or absent. The PA monomers further away from the interface contribute then to the total width of the adsorbed layer. The snapshots of hexadecablock PAs shown in Fig. 5 at small $|\sigma|$ values illustrate such configurations and changes in conformations with growing $|\sigma|$. Note that in Fig. 4A and B the surface charge density is above the adsorption–desorption threshold for all σ values presented.

The two other width indicators reveal a very different behaviour with increasing σ. For $w_{50}(\sigma)$, we often detect a non-monotonic dependence with σ (see Fig. 4C), and no clear scaling for $w_{50}(\sigma)$ variations. This behaviour is consistent with the trends described in ref. 50. We also find that longer charge "blockiness" n along PAs gives rise to larger width w_{50} of the adsorbed layer. Note that the layer widths w_h and w_h^{pos} in the limit of large surface charge densities are dramatically smaller than the w_{50} and the gyration radius; compare the panels of Fig. 4. The quantifiers w_h and w_h^{pos} provide rather local information about PA configurations, because they are based on the width of the first peak of the monomer distributions, $\rho(x)$. This is in contrast to the gyration radius R_g^x that quantifies globally the separation of all PA monomers from the surface. We also observe that as $|\sigma|$ gets reduced further and approaches the adsorption threshold for the chosen conditions, the widths of the adsorbed layer w_h and w_h^{pos} naturally grow and ultimately diverge at $\sigma \to \sigma_c$ (this region is not shown in Fig. 4A and B), see the consideration below and ref. 34 and 35.

C. Critical adsorption conditions: σ_c

Here, we present the results for the PA–surface adsorption–desorption phase transition and compute the dependence $\sigma_c(\kappa)$. We start with Fig. 5 showing the decrease of the PA–surface ES binding energy and typical changes in PA conformations taking place with increasing surface charge density. We find that—particularly for long likely charged blocks in the PA structure such as in Fig. 5A—for highly charged surfaces the ES binding-energy magnitude increases linearly with $|\sigma|$. It reaches—for large PA charge periodicities n, low solution salinities, and large surface charge density—enormous values of $\gtrsim 10^3 k_B T$. In this regime, the positive PA monomers are in a close interface proximity and $|\phi_{ES}| \sim |\sigma|$, as expected from the linear Poisson–Boltzmann theory[34,35] (see eqn (2)). The ES energy of surface-bound PAs then grows linearly with $|\sigma|$, as Fig. 5 shows for highly charged surfaces and diblock PA chains.

One can estimate the ES binding energy E_{ES}^{ext} of a strongly surface-bound diblock PA as the product of all positive monomers with their charge and the ES potential at the distance of

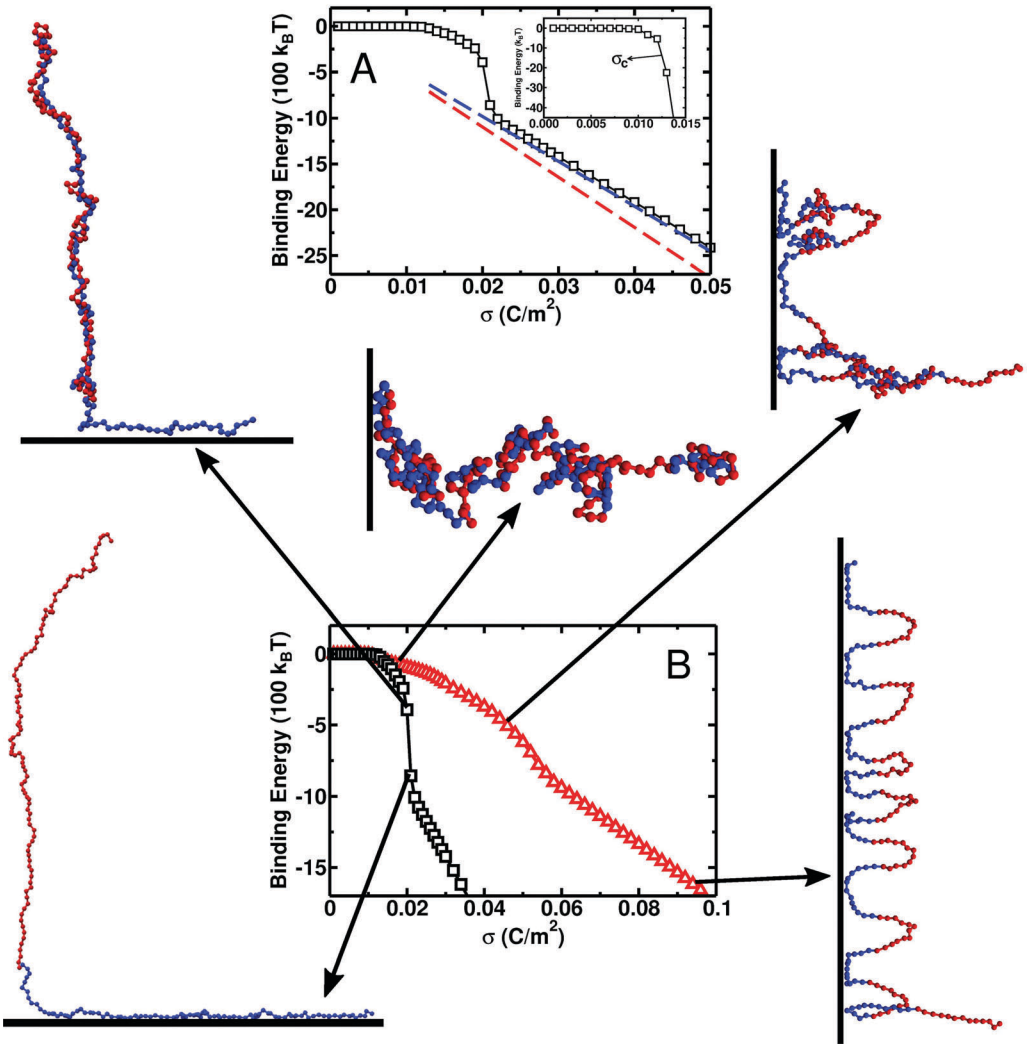

Fig. 5 PA–surface ES binding energy plotted *versus* surface charge density. Panel (A) shows the results for diblock PA chains with n = 104. The inset zooms into the region near the critical transition point, with the critical σ_c value indicated. The linear asymptote (10) computed for $N/2$ monomers for the ES potential at the distance $x = R$ is the dashed red line and that for N_+ = 95 monomers at the maximum of the monomer profile is the dashed blue line (see the text for details). Panel (B) shows the results for n = 104 (black symbols) and n = 13 (red symbols). Large polymer conformational changes are represented by the snapshots coupled to panel (B), evaluated for varying surface charge densities for diblock and hexadecablock PAs. Parameters: N = 208, $n_0 = 10^{-3}$ M.

bead radius from the surface. However, even for very highly charged surfaces some positive monomers are not at the immediate contact with the interface (see *e.g.* the left panels of Fig. 2). Then, a more quantitative way to estimate E_{ES}^{ext} is to fit the number of bound positive monomers (denoted by N_+) and use the ES potential at the peak of $\rho_+(x)$ distribution near the surface, namely

$$E_{ES}^{ext}(\sigma) \approx (N/2)e_0\phi_{ES}[\sigma,x = R] \approx N_+^* e_0\phi_{ES}[\sigma,x = x_{max(\rho+)}]. \quad (10)$$

This latter method with $N_+^* \approx 95$ provides the quantitative agreement for the linear growth of $|E_{ES}^{ext}|$ with $|\sigma|$ observed in our computer simulations for diblock PAs with long stretches of positive charges. The asymptotes (10) are shown in Fig. 5A for n = 104 and N = 208.

The linear $E_{ES}^{ext}(\sigma)$ behaviour in the large-σ limit is interrupted at small surface charge densities, due to severe conformational rearrangements of PA chains (see the conformations linked to Fig. 5B). At small $|\sigma|$ values the oppositely charged blocks within the PA chain are weakly bound to the surface and internally bound to one another by ES attractions, eqn (3). At high surface charge densities, a strong ES binding of the PA's positively charged blocks to the oppositely charged interface takes place. In the course of this abrupt transition, the positive–negative ES contacts between the blocks within the PA are exchanged for external contacts of positive blocks with the negative surface and free negative PA blocks (see Fig. 5A). As we reach the critical adsorption transition, $\sigma \to \sigma_c$, an abrupt decrease in the binding energy takes place (see the inset in Fig. 5A).

For PA chains with shorter block lengths, n = 13 as compared to n = 104, a smoother transition with increasing surface charge density is detected. It is associated with changes of PA shapes from a configuration mostly normal to the surface to "train-and-loop"

conformations parallel to the surface (see Fig. 5B). This figure shows that for shorter block length n along PAs, the decrease in the ES PA–surface binding energy with $|\sigma|$ becomes slower (the red triangles in Fig. 5B). The reason is that the gain in the attractive EB energy of positive PA monomers in the ''trains'' is now diminished by the ES repulsion of negative PA monomers in the ''loops'', which are now rather close to the surface, due to a short block length n. Note also here that for random PAs, see Section 4, the binding energies under the same conditions and surface charge densities are dramatically smaller than for the periodic PAs considered here. The reason is that no binding of consecutive monomer ''trains'' takes place for random PA chains in front of the charged surface.

For calculating the critical adsorption surface charge density σ_c, we implement the algorithm outlined in Section 2 for different values of the PA charge periodicity. Fig. 6A and B illustrate the dependence of $|\sigma_c|$ required for the onset on PA-plane adsorption *versus* solution salinity, the so-called adsorption–desorption transition curve.[34,35] At $|\sigma| < |\sigma_c|$ the PAs are in the desorbed state: the ES attraction to the interface is not strong enough to overcome the entropy losses in delocalised states. Physically, as the Debye screening lengths λ_D get shorter, the ES attraction of positive PA patches to the surface weakens, and the magnitude of $|\sigma_c|$ has to increase to still ensure the PA–surface adsorption. We show in Fig. 6 the results for a set of different lengths $l = (n-1)b$ of alternating patches of positive–negative charges along the PA chains. We systematically vary the salt concentration n_0 and, for each $\kappa \sim \sqrt{n_0}$, we enumerate the value of critical $\sigma_c(\kappa)$ for a given PA length $L = (N-1)b$ and charge periodicity n.

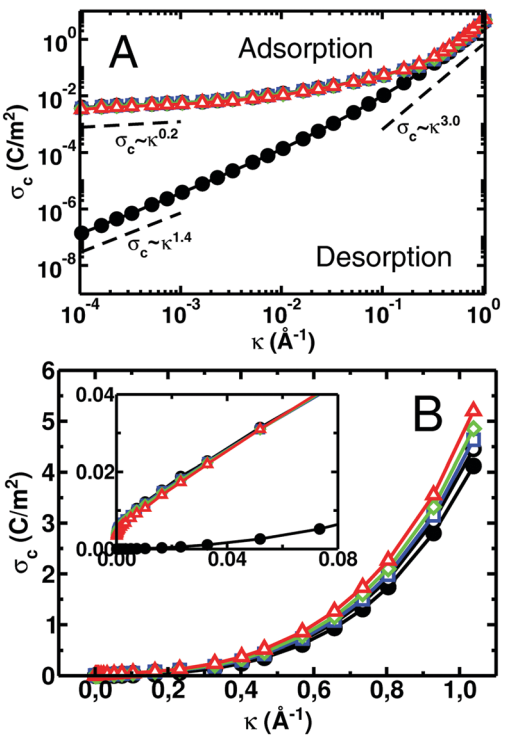

Fig. 6 Critical surface charge density $|\sigma_c|$ for adsorption of PAs with quenched periodic charge distributions, plotted *versus* the reciprocal screening length κ. The charge periodicity is n = 13 (open red), 26 (open green), 52 (open blue), and 104 (open black symbols). The colour scheme is the same as in Fig. 2. For comparison, the data for the adsorption of positively charged PEs of the same length are the filled black circles. The panels (A and B) show the results in the log–log and linear–linear scales, respectively. The inset zooms into the region of low salinities and small σ_c. The simulation time needed to obtain each point of this graph on a standard workstation is about 8 days. Error bars are smaller than the symbol size. Parameters: f = 0, N = 208, and R = 2 Å.

Showing the data in the log–log scale as in Fig. 6A, we identify a rather weak dependence of the critical σ_c on κ at low salinity of the solution,

$$\sigma_{c,PA}(\kappa) \sim \kappa^{0.2}. \quad (11)$$

This scaling is fairly independent of the length of charge patches along the PA chains. In the opposite limit of high salinity—when the respective Debye screening length becomes even shorter than the bead-to-bead distance b_0 along the chain—we observe that

$$\sigma_{c,PA}(\kappa) \sim \kappa^{3}. \quad (12)$$

When the patch length n becomes large, the properties of PA–surface adsorption tend to those for PE–surface adsorption,[34,35,77] as expected. In this limit, the entire long positive patch of the chain is attracted to the surface uniformly along its length, the width of the distribution of surface-adhered PA positive charges $\rho_+(x)$ gets small (see Fig. 2), and thus the value of $|\sigma_c|$ is expected to be reduced dramatically. This is indeed the case, as we exemplify in Fig. 6A and B, where the PE–plane adsorption data are also shown, for the sake of comparison. For PE–surface critical adsorption at low salt we detect a much stronger dependence on solution salinity,

$$\sigma_{c,PE}(\kappa) \sim \kappa^{1.4}, \quad (13)$$

see also ref. 34, 35, 67, 69 and 91, as compared to the weak κ-dependence of eqn (11) for PA–surface adsorption.

One physical reason for this striking difference in PA- *versus* PE–surface critical adsorption at low salt is the ES contribution to the polymer persistence length. The ES-induced stiffening is more pronounced for the PE chains carrying a substantial net charge, as compared to charge-neutral PAs of the same length. For the latter, some ES softening was actually predicted.[9] Particularly pronounced for flexible PAs, a given monomer on the PA chain is on average surrounded more often by oppositely charged monomers and the resulting correlation-induced dipole–dipole interactions[104] give rise to a negative ES term in the persistence length, so that $l_{p,ES}^{PA} < 0$.[9,112] We remind the reader that—depending on the bare PE persistence length—for the ES contribution the scaling relations $l_{p,ES}^{PE}(\kappa) \sim \kappa^{-1}$ and $l_{p,ES}^{PE}(\kappa) \sim \kappa^{-2}$ exist for the flexible and semiflexible (rod-like) chains, respectively.[32,35,113,115]

We find that, as the periodicity of alternating patches of charges n along the PA increases, the corresponding critical surface charge density σ_c decreases slightly but systematically. This effect is visible at intermediate-to-high salinities in the linear-scale plot of Fig. 6B. Physically, longer alternating blocks

of positive and negative charges along the chain will enable the polymer to displace the negative patches further away from the negative surface attracting positive PA patches (see also ref. 114). This, in turn, will help in reducing the magnitude of $|\sigma_c|$ necessary for PA–surface adsorption driven by ES attraction of positive PA monomers.

IV. Random PA charge distributions

In this section, we present the results and clarify the differences for monomer distribution profiles, adsorbed-layer width, and critical adsorption conditions for the PA chains with random—rather than periodic—distribution of charges. The results shown are averaged over $M = 30$ different random PA charge distributions, generated according to the algorithm in Section 2. This averaging is vital to get the statistically meaningful results, but it requires considerable simulation times. For instance, the simulation time for each point of Fig. 10 is about 2 months on a single-core computer.

Let us summarise here some basic trends known for surface adsorption of randomly charged PA chains, at varying surface charge density σ. For non-screened PA-plane interactions, the width w_{PA} can vary non-monotonically with σ (see ref. 1). For weakly charged surfaces, the "pole" regime for PA adsorption is realised (stretched chains),[4,43,44,51] with the PA layer thickness predicted to increase with $|\sigma|$ value. In this regime, the Gouy–Chapman length λ_{GC} (8) is much larger than the size of an unperturbed PA coil.[4] In the intermediate "fence" regime (folded stretched PAs) and strong-adsorption "pancake" regimes,[4,43] the ES attractions of the oppositely charged PA monomers to the surface get stronger. They are counter-balanced by the entropic free energy of loops extending into the solution. The Gouy–Chapman length λ_{GC} in these limits is as short as the polymer size or inter-charge distances, respectively.[4] For highly charged surfaces, the PA layer thickness in the "pancake" regime only weakly depends on chain polymerisation degree N and surface charge density $|\sigma|$, being determined by the length of the polymer loops formed between the adsorbed PA fragments[1] (see also Fig. 1 and 5). The surface charge densities for the "pole" and "fence" regimes were predicted theoretically to scale as $\sigma_{pole}(N) \sim N^{-1}$ and $\sigma_{fence}(N) \sim N^{-3/4}$, whereas in the "pancake" adsorption regime no dependence on the chain length is expected.[4] Note that theories of PA–surface adsorption often assume the Gaussian monomer statistics, with weak perturbations by ES attachment to the surface.

A. Monomer density profiles $\rho_{\pm}(x)$

The distribution of PA monomers in the vicinity of a negatively charged surface, $\rho_+(x) + \rho_-(x)$, computed in our simulations is presented in Fig. 7. We observe that with increasing surface charge density the first peak near the interface becomes more pronounced and gets narrower; compare the curves in Fig. 7. In this plot, the values of w_h are shown by the horizontal lines for $\sigma = -0.01$ C m^{-2} and -0.03 C m^{-2}.

B. Adsorbed layer width w

The widths $w_h(\sigma)$ and $w_h^{pos}(\sigma)$ of the adsorbed PA layer in their dependence on σ are shown in Fig. 8A and B. The layer thickness

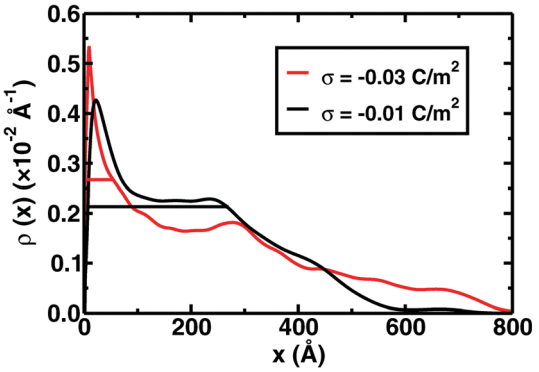

Fig. 7 Monomer distribution profiles, $\rho_+(x) + \rho_-(x)$, for adsorption of random PAs onto a charged plane (above the adsorption threshold). The charge density is $\sigma = -0.01$ C m^{-2} (black) and -0.03 C m^{-2} (red curve), $f = 0$, $N = 208$, $n_0 = 10^{-5}$ M or $\lambda_D \approx 960$ Å.

is computed at the half-height of the PA monomer density profile (above the adsorption threshold). We find that the layer width w_h decreases with the surface charge density $|\sigma|$. This trend is consistent with progressive accumulation of PA monomers near the surfaces with a higher charge density, as for the case of periodic PAs (see Fig. 4). It is also in agreement with the previous findings (see *e.g.* Fig. 9 in ref. 1).

Similar trends exist for the $w_h^{pos}(\sigma)$ dependence shown in Fig. 8B: positively charged PA monomers are localised stronger near the surfaces possessing higher charges. The general trend is that for low $|\sigma|$ values the adsorbed layer widths w_h and w_h^{pos} for random PAs are smaller than for periodic PAs, with the shortest periodicity considered here of $n = 13$ (see the red triangles in Fig. 8). The periodic PAs in the adsorbed state stay mainly parallel to the surface, whereas random PAs form large loops dangling in the solution at distances $\gtrsim \lambda_D$, giving rise to a larger width of the adsorbed layer; compare the snapshots in Fig. 5 and 9. For highly charged surfaces, however, the adsorbed layer of random PAs is thicker than for periodic PAs; compare the curves in Fig. 8A and B.

The adsorbed layer width can also be estimated as the distance from the plane up to which 50% of PA monomers are located, w_{50}, and from the polymer gyration radius normal to the surface, R_g^x, as demonstrated in Fig. 8C and D. The latter definition yields, on the contrary, that the adsorbed layer width grows with increasing $|\sigma|$. This is reminiscent of the results of Fig. 4D for periodic PA chains (note, however, the different maximal σ values for these two plots). To explain this observation, we refer the reader to Fig. 7 that shows that with increasing surface charge density, an extension of the monomer profile away from the surface takes place, in addition to a sharper maximum of the first $\rho_+(x) + \rho_-(x)$ peak near the plane. This polymer extension promotes an increase in R_g^x and, thus, yields larger adsorbed layer thickness in terms of the gyration radius. Note that R_g^x yields similar trends for both periodic and random PAs.

Similarly to the layer width assessed by computing the values of w_h and w_h^{pos}, at moderate and high surface charge densities the width estimators w_{50} and R_g^x for random PAs are larger than those for periodic PAs. Note that charge-neutral random PAs are

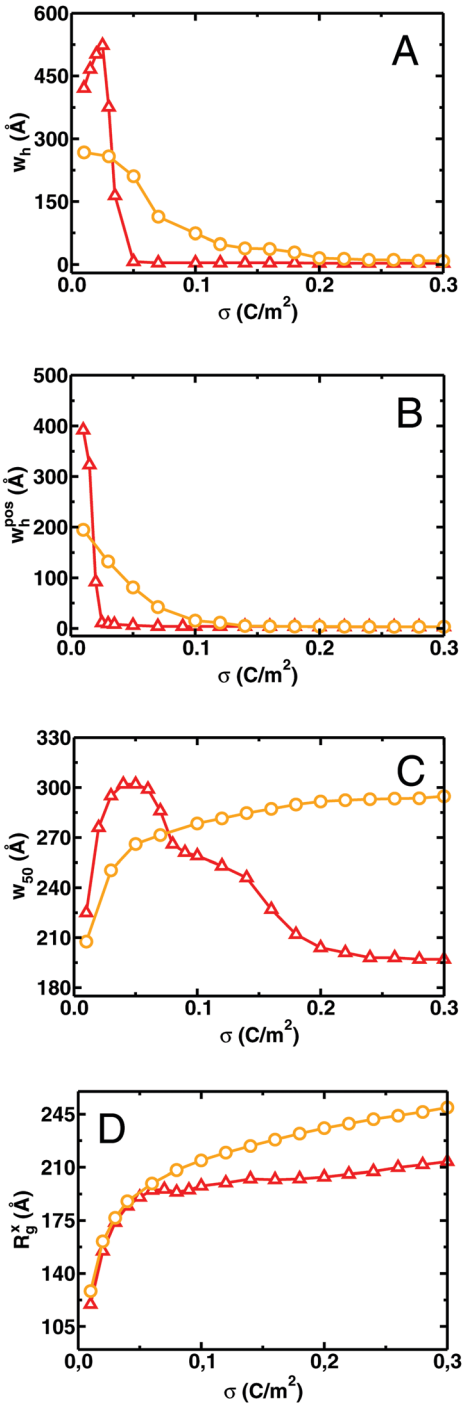

Fig. 8 Width of surface-adsorbed layers of random PAs (orange circles) *versus* surface charge density magnitude, $|\sigma|$. Panels (A and B) show the layer width at 1/2 of the height computed from the distributions of all monomers and evaluated from the $\rho_+(x)$ profiles only. Panel (C) shows the width of the adsorbed layer which contains 50% of all the PA monomers. Panel (D) shows the chain's gyration radius (normal to the surface). Parameters are the same as in Fig. 7. The results for periodic PAs with n = 13 from Fig. 4 are shown as the red triangles. Note that the maximal $|\sigma|$ value here is 3 times larger than in Fig. 4.

rather compact in solution and the ES interactions with a charged surface deform and stretch their coils (the "pole" regime) until σ reaches the value above which the behaviour gets inverted, the so-called "fence" regime (see ref. 1, 4, 43, 44 and 57 for a detailed picture of PA–surface adsorption regimes).

In Fig. 9 we show some representative conformations of random-charge net-neutral PAs for growing surface charge densities $|\sigma|$. When computing the PA–surface ES binding energy, we find that both the number of PA–surface contacts and their binding energy increase for more highly charged surfaces. Note that the linear growth of the absolute value of the ES binding energy with $|\sigma|$ for random PAs is much slower as compared to periodic PAs, even for the shortest charge periodicity (see the red triangle in Fig. 9 for the n = 13 case).

C. Critical adsorption conditions σ_c

Fig. 10 illustrates the critical surface charge density $|\sigma_c|$ *versus* the solution salinity required for the adsorption of PAs with quenched random charge distributions (the orange circles). The dependence $\sigma_c(\kappa)$ exhibits similar trends and close values as for periodic PAs with the shortest periodicity of n = 13 (the red triangles in Fig. 10 are for the hexadecablock chain). Random PAs have statistically very short charge blocks, irregularly distributed along the polymer.

For large solution salinities, we observe somewhat larger critical σ_c values needed for adsorption of random PAs, as compared to periodic PAs. For small κ values, however, random PAs require somewhat smaller $|\sigma_c|$ for critical adsorption, with respect to charge-periodic PA chains; compare the data sets in Fig. 10. This behaviour is consistent with the variations of the layer widths w_h, w_h^{pos}, and w_{50} with growing surface charge density σ, as computed for charge-periodic and random PAs in Fig. 8A–C. The critical PA–surface adsorption curves in Fig. 6 and 10 are the main results of this study.

The repulsion of negative PA monomers from the negatively charged surface at low salt leads to the formation of large loops, which pull/displace positive PA monomers away from the surface (see Fig. 9). This can be one reason for somewhat larger $|\sigma_c|$ values obtained for periodic PAs with longer blocks at low salt (see Fig. 10). As random PAs can be considered as polymer chains having very short and irregular charge blocks, ordered loops are formed rarely and the critical surface charge density at low salt is smaller than for periodic PAs (see Fig. 10). Note that for random PAs, the increase in $|\sigma|$ leads to a decreasing loop length in the "fence" regime and reaches the "pancake" limit.[4] For periodic PAs, the loop length increases with $|\sigma|$ and reaches saturation when the loops cannot stretch anymore.

Another probable physical reason for these σ_c differences between periodic and random PAs can be that at very small n_0 the periodic PA chains—when free in the solution—are strongly complexed internally. Namely, the positive and negative blocks form rather ordered, folded structures, see the top left image in Fig. 5. The longer the block length, the stronger and more ordered this internal ES-driven complexation is (in the low-salt limit). When such an internally folded PA approaches the charged interface, the internal ES contacts need to be disrupted. To ensure this for longer PA charge periodicities n, larger surface

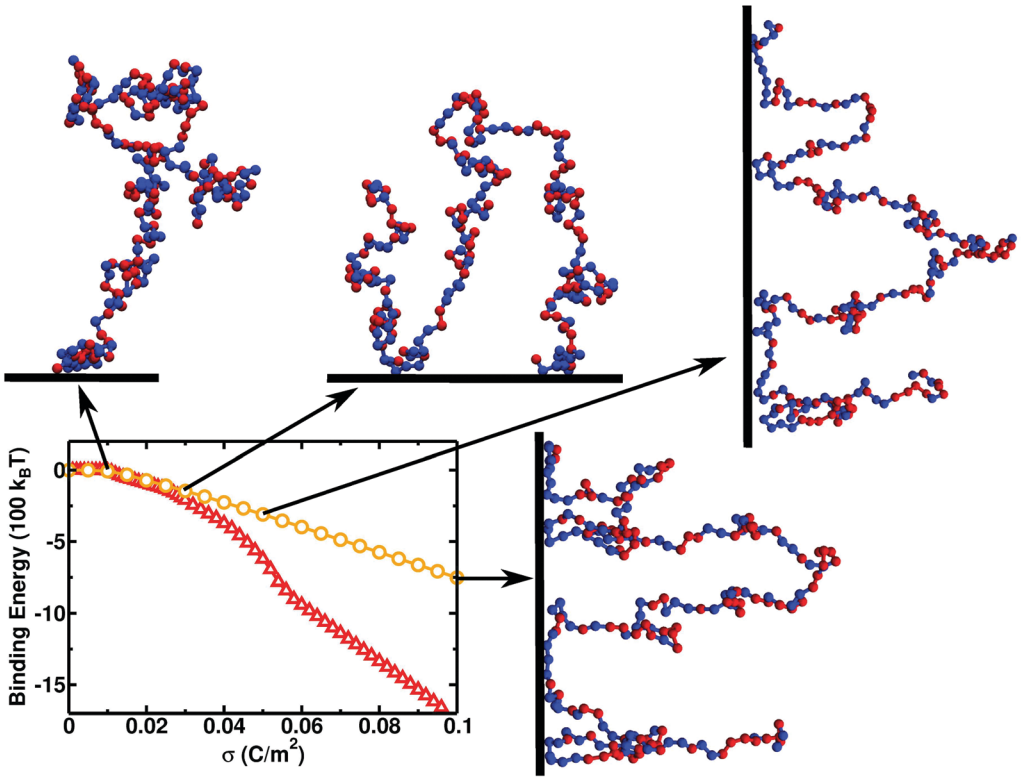

Fig. 9 ES binding energy of random PAs to the negatively charged plane (orange circles) *versus* surface charge density, with significant PA conformational changes illustrated. The data for periodic PAs with n = 13 are the red triangles. Parameters: N = 208 and $n_0 = 10^{-3}$ M ($\lambda_D \approx 96$ Å).

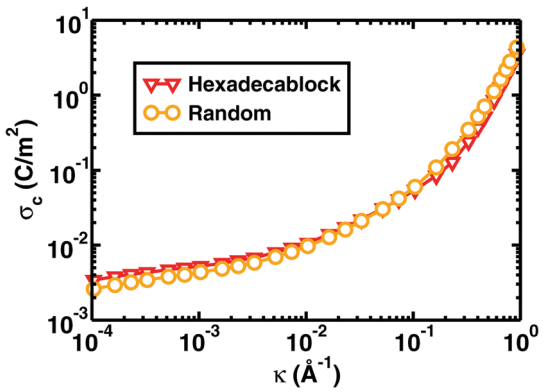

Fig. 10 Critical charge density $|\sigma_c|$ for adsorption of PAs with random charge distribution (orange circles) onto a plane, plotted *versus* κ. The data for PAs with periodic charges at n = 13 (hexadecablock polymers with N = 208) are the red triangles. Parameters are the same as in Fig. 7.

charge densities are needed. This can describe the order of the low-salt curves in Fig. 6 and smaller values of σ_c for random PAs as compared to the periodic ones in the low-salt regime (see Fig. 10).

In the limit of very high salt, on the contrary, the ES interactions within the PA chains are strongly screened and the differences in the critical surface charge densities can be due to differently restricted entropic freedom of the PA chains upon adsorption.

V. Discussion and conclusions

We performed Metropolis Monte Carlo computer simulations aimed at investigating the properties of ES-driven adsorption of flexible PA chains with periodic and random charge distributions onto charged planar surfaces. The PA chains that are charge-neutral form rather compact structures in the solution and the ES interactions with the surface stretch and polarise the chain, stabilising thereby the adsorbed state. Different ways to define the width of the adsorbed layer used above (Fig. 4) have shown that increasing $|\sigma|$ leads to accumulation of positive PA monomers near the surface, but concurrently gives rise to more stretched chains in terms of the gyration radius. In comparison to random PA chains—for which in the low-salt limit the "pole", "fence" and "pancake" regimes are known to occur[1,4,43]—for regular periodic PAs the adsorption onto the charged surface was typically considerably stronger. Diblock PAs have a larger ES binding energy: such chains are most extended in the solution and most condensed onto the interface, as compared to multi-block PAs. The differences in the PA–surface ES association energy were even more dramatic if diblock PAs are compared to random PAs (Fig. 5 and 9).

Our findings for the critical adsorption conditions revealed a number of new features for both periodic and random PA chains (Fig. 6 and 10). We showed that increasing PA block length enhances the adsorption and accordingly $|\sigma_c|$ gets reduced at large salt concentrations (but not at small n_0). We detected a weak dependence of σ_c on the solution salinity,

namely $\sigma_c(\kappa) \sim \kappa^{0.2}$, for both periodic and random PAs at low ionic strengths. Similar weak dependence of $|\sigma_c|$ on the reciprocal Debye length was also observed for PE adsorption onto dipolar net-neutral spherical Janus nanoparticles.[79] We also found that at high salinities—when the corresponding Debye lengths become shorter than monomer–monomer distances—the PA adsorption reveals the same scaling behaviour as for PE critical adsorption onto the oppositely charged plane, namely $\sigma_c(\kappa) \sim \kappa^3$.[34,35,67]

In future simulation-based studies of PA–surface adsorption several additional effects can be included. First, similar to PE–surface adsorption,[80] the implications of a low dielectric permittivity below the adsorbing interface[118] can be considered.[80] Second, the effects of varying PA linear charge density e_0/b_0 and counterion condensation onto the polymer and charged surface can be investigated. For this, the compensation fractions and the effective charge densities need to be self-consistently computed for the plane and linear chain. Third, the adsorption of PAs with annealed charge distribution and titratable groups can be studied.[117,119] The value of $|\sigma_c|$ for this case is expected to be smaller because the PA charge pattern can adjust, in order to enhance the PA–surface ES attraction. This, in turn, will reduce $|\sigma_c|$. Fourth, the length of the PA charge patches can be a random variable drawn from a particular distribution. One can consider power law, exponential, or Rayleigh-like forms, $p(n) = 2n \exp[-n^2/\langle n^2\rangle]/\langle n^2\rangle$, with $\langle n^2\rangle$ being the average block length. The chains constructed in this way will feature a mixture of surface-adsorption properties of both periodic and random PAs considered above. Then, additional ensemble averaging over independent realisations of PA charge patterns needs to be performed, in order to obtain reliable results for the adsorbed layer width and $|\sigma_c|$. Fifth, the implications of varying PA length on critical adsorption for both periodic and random chains can be elucidated. The results are then to be compared with the theoretical predictions for PA–surface adsorption charge density, decreasing for long chains as[4] $|\sigma(N)| \sim N^{-3/4}$ (in the "fence" regime) and expected to be only weakly dependent on the chain length at strong screening. Finally, one can compute the amount Γ of adsorbed PAs per unit surface area, see *e.g.* ref. 42 and 46 for the experimental data on gelatin coverage of mica surfaces and gold particles.[121] This requires explicit simulations of multi-chain adsorption[44] with finite PA concentrations in the bulk,[44] salt-dependent intra-chain ES interactions, and PA–surface adsorption isotherm[43,54] to be determined. All these experimentally important interrelations require systematic large-scale simulations, the subject of our future research.

Lastly, we believe that our simulation-based analysis of critical PA–surface adsorption conditions will help in elucidating the properties of protein denaturation and unfolding triggered by adsorption onto charged interfaces.[24]

Conflicts of interest

There are no conflicts to declare.

Acknowledgements

Computer resources were supplied by the Center for Scientific Computing (NCC/GridUNESP) of the Sao Paulo State University (UNESP). D. L. Z. C. acknowledges the Sao Paulo Research Foundation (FAPESP, Process Grant No. 2013/13151-7) for financial support.

References

1 A. V. Dobrynin, R. H. Colby and M. Rubinstein, Polyampholytes, *J. Polym. Sci., Part B: Polym. Phys.*, 2004, **42**, 3513.
2 P. G. Higgs and J.-F. Joanny, Theory of polyampholyte solutions, *J. Chem. Phys.*, 1991, **94**, 1543.
3 J.-F. Joanny, Adsorption of a polyampholyte chain, *J. Phys. II*, 1994, **4**, 1281.
4 A. V. Dobrynin, M. Rubinstein and J.-F. Joanny, Adsorption of a polyampholyte chain on a charged surface, *Macromolecules*, 1997, **30**, 4332.
5 A. V. Dobrynin, Polyampholyte adsorption on a charged sphere, *Phys. Rev. E: Stat., Nonlinear, Soft Matter Phys.*, 2001, **63**, 051802.
6 S. E. Kudaibergenov, Polyampholytes, *Encyclopedia of Polymer Science and Technology*, John Wiley & Sons, 2002.
7 R. R. Netz and D. Andelman, Neutral and charged polymers at interfaces, *Phys. Rep.*, 2003, **380**, 1.
8 I. Borukhov, D. Andelman and H. Orland, Random polyelectrolytes and polyampholytes in solution, *Eur. Phys. J. B*, 1998, **5**, 869.
9 B.-Y. Ha and D. Thirumalai, Persistence length of intrinsically stiff polyampholyte chains, *J. Phys. II*, 1997, **7**, 88.
10 *Paper Chemistry*, ed. T. Lindstrom and J. C. Roberts, Blackie, London, 1991.
11 J. A. Wolff, J. E. Hagstrom, V. G. Budker and V. S. Trubetskoy, *Polyampholytes for delivering polyions to a cell*, *US Pat.*, US 6383811 B2, 2009.
12 S. Müller-Späth, *et al.*, Charge interactions can dominate the dimensions of intrinsically disordered proteins, *Proc. Natl. Acad. Sci. U. S. A.*, 2010, **107**, 14609.
13 R. K. Das and R. V. Pappu, Conformations of intrinsically disordered proteins are influenced by linear sequence distributions of oppositely charged residues, *Proc. Natl. Acad. Sci. U. S. A.*, 2013, **110**, 13392.
14 Y. Kantor, H. Li and M. Kardar, Conformations of polyampholytes, *Phys. Rev. Lett.*, 1992, **69**, 61.
15 Y. Kantor, M. Kardar and H. Li, Statistical mechanics of polyampholytes, *Phys. Rev. E: Stat. Phys., Plasmas, Fluids, Relat. Interdiscip. Top.*, 1994, **49**, 1383.
16 A. V. Dobrynin and M. Rubinstein, Flory theory of a polyampholyte chain, *J. Phys. II*, 1995, **5**, 677.
17 A. M. Gutin and E. I. Shakhnovich, Effect of a net charge on the conformation of polyampholytes, *Phys. Rev. E: Stat. Phys., Plasmas, Fluids, Relat. Interdiscip. Top.*, 1994, **50**, R3322.
18 A. Yu. Grosberg, Disordered polymers, *Phys.-Usp.*, 1997, **40**, 125.

19 S. F. Edwards, P. R. King and P. Pincus, Phase changes in polyampholytes, *Ferroelectrics*, 1980, **30**, 3.

20 M. Milik and J. Skolnick, Insertion of peptide chains into lipid membranes: an off-lattice Monte Carlo dynamics model, *Proteins*, 1993, **15**, 10.

21 H. Khandelia, J. H. Ipsen and O. G. Mouritsen, The impact of peptides on lipid membranes, *Biochim. Biophys. Acta, Biomembr.*, 2008, **1778**, 1528.

22 M. O. Jensen, O. G. Mouritsen and G. H. Peters, Simulations of a membrane-anchored peptide: structure, dynamics and influence on bilayer properties, *Biophys. J.*, 2004, **86**, 3556.

23 V. G. Contessoto, V. M. de Oliveira, S. J. de Carvalho, L. C. Oliveira and V. B. P. Leite, NTL9 folding at constant pH: the importance of electrostatic interaction and pH-dependence, *J. Chem. Theory Comput.*, 2016, **12**, 3270.

24 S. J. de Carvalho, *et al.*, *Protein unfolding by attractive surfaces*, 2017, work in preparation.

25 A. V. Dobrynin and M. Rubinstein, Theory of polyelectrolytes in solutions and at surfaces, *Prog. Polym. Sci.*, 2005, **30**, 1049.

26 J.-M. Y. Carrillo and A. V. Dobrynin, Molecular dynamics simulations of polyelectrolyte adsorption, *Langmuir*, 2007, **23**, 2472.

27 R. Messina, Electrostatics in soft matter, *J. Phys.: Condens. Matter*, 2009, **21**, 113102.

28 H. Boroudjerdi, Y.-W. Kim, A. Naji, R. R. Netz, X. Schlagberger and A. Serr, Statics and dynamics of strongly charged soft matter, *Phys. Rep.*, 2005, **416**, 129.

29 I. Szilagyi, G. Trefalt, A. Tiraferri, P. Maroni and M. Borkovec, Polyelectrolyte adsorption, interparticle forces, and colloidal aggregation, *Soft Matter*, 2014, **10**, 2479.

30 A. Takuhashi and M. Kawaguchi, The structure of macromolecules adsorbed on interfaces, *Adv. Polym. Sci.*, 1982, **46**, 1.

31 J. Meadows, *et al.*, Characterization of the adsorption–desorption behavior of hydrolyzed polyacrylamide, *J. Colloid Interface Sci.*, 1989, **132**, 319.

32 J. L. Barrat and J.-F. Joanny, Theory of polyelectrolyte solutions, in *Adv. Chem. Phys.*, ed. I. Prigogine and S. A. Rice, 1996, vol. 94, p. 1.

33 A. B. Kayitmazer, *et al.*, Protein-polyelectrolyte interactions, *Soft Matter*, 2013, **9**, 2553.

34 A. G. Cherstvy and R. G. Winkler, Polyelectrolyte adsorption onto oppositely charged interfaces: unified approach for plane, cylinder, and sphere, *Phys. Chem. Chem. Phys.*, 2011, **13**, 11686.

35 R. G. Winkler and A. G. Cherstvy, Strong and weak polyelectrolyte adsorption onto oppositely charged curved surfaces, *Adv. Polym. Sci.*, 2014, **255**, 1.

36 J. H. E. Hone, A. M. Howe and T. H. Whitesides, Rheology of polystyrene latexes with adsorbed and free gelatin, *Colloids Surf., A*, 2000, **162**, 283.

37 B. Mahltig, H. Walter, C. Harrats, P. Müller-Buschbaum, R. Jéroümeb and M. Stamm, Adsorption of polyampholyte copolymers at the solid/liquid interface: the influence of pH and salt on the adsorption behaviour, *Phys. Chem. Chem. Phys.*, 1999, **1**, 3853.

38 Y. Tran, P. Perrin, S. Deroo and F. Lafuma, Adsorption of randomly annealed polyampholytes at the silica-water interface, *Langmuir*, 2006, **22**, 7543.

39 T. Kato, M. Kawaguchi, A. Takahashi, T. Onabe and H. Tanaka, Adsorption of sulfobetaine polyampholyte on silica surfaces from aqueous salt solutions, *Langmuir*, 1999, **15**, 4302.

40 F. L. Berre, M. Malmsten and E. Blomberg, Interfacial properties of a model polyampholyte studied by surface force measurements, ESCA, and ellipsometry, *Langmuir*, 2001, **17**, 699.

41 N. Kawanishi, H. K. Christenson and B. W. Ninham, Measurement of the interaction between adsorbed polyelectrolytes: gelatin on mica surfaces, *J. Phys. Chem.*, 1990, **94**, 4611.

42 Y. Kamiyama and J. Israelachvili, Effect of pH and salt on the adsorption and interactions of an amphoteric polyelectrolyte, *Macromolecules*, 1992, **25**, 5081.

43 E. B. Zhulina, A. V. Dobrynin and M. Rubinstein, Adsorption of a polyampholyte on a charged spherical particle, *Eur. Phys. J. E: Soft Matter Biol. Phys.*, 2001, **5**, 41.

44 A. V. Dobrynin, S. P. Obukhov and M. Rubinstein, Long-range multichain adsorption of polyampholytes on a charged surface, *Macromolecules*, 1999, **32**, 5689.

45 H. Schiessel and A. Blumen, Conformations of freely jointed polyampholytes in external fields, *J. Chem. Phys.*, 1996, **104**, 6036.

46 D. Eck, C. A. Helm, N. J. Wagner and K. A. Vaynberg, Plasmon resonance measurements of the adsorption and adsorption kinetics of a biopolymer onto gold nanocolloids, *Langmuir*, 2001, **17**, 958.

47 V. V. Palyulin, T. Ala-Nissila and R. Metzler, Polymer translocation: the first two decades and the recent diversification, *Soft Matter*, 2014, **10**, 9016.

48 E. Ercolini, F. Valle, J. Adamcik, G. Witz, R. Metzler, P. de los Rios, J. Roca and G. Dietler, Fractal dimension and localization of DNA knots, *Phys. Rev. Lett.*, 2007, **98**, 058102.

49 J. Adamcik, J.-H. Jeon, K. J. Karczewski, R. Metzler and G. Dietler, Quantifying supercoiling-induced denaturation bubbles in DNA, *Soft Matter*, 2012, **8**, 8651.

50 M. O. Khan, T. Akesson and B. Jönsson, Adsorption of polyampholytes to charged surfaces, *Macromolecules*, 2001, **34**, 4216.

51 R. R. Netz and J.-F. Joanny, Complexation behavior of polyampholytes and charged objects, *Macromolecules*, 1998, **31**, 5123.

52 A. V. Dobrynin, S. P. Obukhov and M. Rubinstein, Long-range multichain adsorption of polyampholytes on a charged surface, *Macromolecules*, 1999, **32**, 5689.

53 Y. Levin and M. C. Barbosa, Conformational phase transition of a polyampholyte in a low dielectric solvent, *Europhys. Lett.*, 1995, **31**, 513.

54 E. B. Zhulina, A. V. Dobrynin and M. Rubinstein, Adsorption isotherms of polyampholytes at charged spherical particles, *J. Phys. Chem. B*, 2001, **105**, 8917.

55 B. Mahltig, J.-F. Gohy, R. Jerome, G. Pfütze and M. Stamm, Desorption behaviour of regular adsorbed polyampholytic layers, *J. Polym. Res.*, 2003, **10**, 69.

56 Y. Tran, P. Perrin, S. Deroo and F. Lafuma, Adsorption of randomly annealed polyampholytes at the silica-water interface, *Langmuir*, 2006, **22**, 7543.

57 A. V. Dobrynin, E. B. Zhulina and M. Rubinstein, Structure of adsorbed polyampholyte layers at charged objects, *Macromolecules*, 2001, **34**, 627.

58 A. V. Dobrynin, M. Rubinstein and J.-F. Joanny, Polyampholyte solutions between charged surfaces: Debye–Hückel theory, *J. Chem. Phys.*, 1998, **109**, 9172.

59 T. Soddemann, H. Schiessel and A. Blumen, Molecular-dynamics simulations of polyampholytes: instabilities due to excess charges and external fields, *Phys. Rev. E: Stat. Phys., Plasmas, Fluids, Relat. Interdiscip. Top.*, 1998, **57**, 2081.

60 S. Ulrich, M. Seijo and S. Stoll, A Monte Carlo study of weak polyampholytes: stiffness and primary structure influences on titration curves and chain conformations, *J. Phys. Chem. B*, 2007, **111**, 8459.

61 A. Akinchina, N. P. Shusharina and P. Linse, Diblock polyampholytes grafted onto spherical particles: Monte Carlo simulation and lattice mean-field theory, *Langmuir*, 2004, **20**, 10351.

62 A. Akinchina and P. Linse, Diblock polyampholytes grafted onto spherical particles: effect of stiffness, charge density, and grafting density, *Langmuir*, 2007, **23**, 1465.

63 R. Messina, Behavior of block-polyampholytes near a charged surface, *Eur. Phys. J. E: Soft Matter Biol. Phys.*, 2007, **22**, 325.

64 D. L. Z. Caetano and S. J. de Carvalho, Conformational properties of block-polyampholytes adsorbed on charged cylindrical surfaces, *Eur. Phys. J. E: Soft Matter Biol. Phys.*, 2017, **40**, 33.

65 J. Jeon and A. V. Dobrynin, Monte Carlo simulations of polyampholyte-polyelectrolyte complexes: effect of charge sequence and strength of electrostatic interactions, *Phys. Rev. E: Stat., Nonlinear, Soft Matter Phys.*, 2003, **67**, 061803.

66 S. Ulrich, M. Seijo, F. Carnal and S. Stoll, Formation of complexes between nanoparticles and weak polyampholyte chains. Monte Carlo simulations, *Macromolecules*, 2011, **44**, 1661.

67 F. W. Wiegel, Adsorption of a macromolecule to a charged surface, *J. Phys. A: Math. Gen.*, 1977, **10**, 299.

68 F. W. Wiegel, *Introduction to Path-Integral Methods in Physics and Polymer Science*, World Scientific, Singapore, 1986.

69 M. Muthukumar, Adsorption of a polyelectrolyte chain to a charged surface, *J. Chem. Phys.*, 1987, **86**, 7230.

70 A. V. Dobrynin, Theory and simulations of charged polymers: from solution properties to polymeric nanomaterials, *Curr. Opin. Colloid Interface Sci.*, 2008, **13**, 376.

71 F. von Goeler and M. Muthukumar, Adsorption of polyelectrolytes onto curved surfaces, *J. Chem. Phys.*, 1994, **100**, 7796.

72 M. Muthukumar, Pattern recognition by polyelectrolytes, *J. Chem. Phys.*, 1995, **103**, 4723.

73 P. Linse, Adsorption of weakly charged polyelectrolytes at oppositely charged surfaces, *Macromolecules*, 1996, **29**, 326.

74 I. Borukhov, D. Andelman and H. Orland, Scaling laws of polyelectrolyte adsorption, *Macromolecules*, 1998, **31**, 1665.

75 R. R. Netz and J.-F. Joanny, Adsorption of semiflexible polyelectrolytes on charged planar surfaces: charge compensation, charge reversal, and multilayer formation, *Macromolecules*, 1999, **32**, 9013.

76 A. Shafir, D. Andelman and R. R. Netz, Adsorption and depletion of polyelectrolytes from charged surfaces, *J. Chem. Phys.*, 2003, **119**, 2355.

77 S. J. de Calvalho, R. Metzler and A. G. Cherstvy, Critical adsorption of polyelectrolytes onto planar and convex highly charged surfaces: the nonlinear Poisson-Boltzmann approach, *New J. Phys.*, 2016, **18**, 083037.

78 S. J. de Carvalho, First-order-like transition in salt-induced macroion-polyelectrolyte desorption, *Europhys. Lett.*, 2010, **92**, 18001.

79 S. J. de Carvalho, R. Metzler and A. G. Cherstvy, Critical adsorption of polyelectrolytes onto charged Janus nanospheres, *Phys. Chem. Chem. Phys.*, 2014, **16**, 15539.

80 A. G. Cherstvy and R. G. Winkler, Polyelectrolyte adsorption onto oppositely charged interfaces: image-charge repulsion and surface curvature, *J. Phys. Chem. B*, 2012, **116**, 9838.

81 E. Gurovitch and P. Sens, Adsorption of polyelectrolyte onto a colloid of opposite charge, *Phys. Rev. Lett.*, 1999, **82**, 339.

82 K. K. Kunze and R. R. Netz, Salt-induced DNA-histone complexation, *Phys. Rev. Lett.*, 2000, **85**, 4389.

83 R. R. Netz and J.-F. Joanny, Complexation between a semiflexible polyelectrolyte and an oppositely charged sphere, *Macromolecules*, 1999, **32**, 9026.

84 A. G. Cherstvy and R. G. Winkler, Strong and weak adsorptions of polyelectrolyte chains onto oppositely charged spheres, *J. Chem. Phys.*, 2006, **125**, 064904.

85 R. G. Winkler and A. G. Cherstvy, Critical adsorption of polyelectrolytes onto charged spherical colloids, *Phys. Rev. Lett.*, 2006, **96**, 066103.

86 R. G. Winkler and A. G. Cherstvy, Adsorption of weakly charged polyelectrolytes onto oppositely charged spherical colloids, *J. Phys. Chem. B*, 2007, **111**, 8486.

87 H. Boroudjerdi, A. Naji and R. R. Netz, Global analysis of the ground-state wrapping conformation of a charged polymer on an oppositely charged nano-spheres, *Eur. Phys. J. E: Soft Matter Biol. Phys.*, 2014, **37**, 21.

88 J. Gross, T. Vogel and M. Bachmann, Structural phases of adsorption for flexible polymers on nanocylinder surfaces, *Phys. Chem. Chem. Phys.*, 2015, **17**, 3070.

89 S. J. de Carvalho and D. L. Z. Caetano, Adsorption of polyelectrolytes onto oppositely charged cylindrical macroions, *J. Chem. Phys.*, 2013, **138**, 244909.

90 V. M. de Oliveira and S. J. de Carvalho, Adsorption of pH-responsive polyelectrolyte chains onto spherical macroions, *Eur. Phys. J. E: Soft Matter Biol. Phys.*, 2014, **37**, 75.

91 S. J. de Carvalho, R. Metzler and A. G. Cherstvy, Inverted critical adsorption of polyelectrolytes in confinement, *Soft Matter*, 2015, **11**, 4430.

92 A. G. Cherstvy, Critical Polyelectrolyte adsorption under confinement: planar slit, cylindrical pore, and spherical cavity, *Biopolymers*, 2012, **97**, 311.

93 H. R. Shojaei and M. Muthukumar, Adsorption and encapsulation of flexible polyelectrolytes in charged spherical vesicles, *J. Chem. Phys.*, 2017, **146**, 244901.

94 J. McNamara, C. Y. Kong and M. Muthukumar, Monte Carlo studies of adsorption of a sequenced polyelectrolyte to patterned surfaces, *J. Chem. Phys.*, 2002, **117**, 5354.

95 R. M. Adar, D. Andelman and H. Diamant, Electrostatics of patchy surfaces, *Adv. Colloid Interface Sci.*, 2017, submitted.

96 J. Forsman, Polyelectrolyte adsorption: electrostatic mechanisms and nonmonotonic responses to salt addition, *Langmuir*, 2012, **28**, 5138.

97 G. S. Manning, The molecular theory of polyelectrolyte solutions with applications to the electrostatic properties of polynucleotides, *Q. Rev. Biophys.*, 1978, **11**, 179.

98 G. Reddy, R. Chang and A. Yethiraj, Adsorption and dynamics of a single polyelectrolyte chain near a planar charged surface: Molecular Dynamics simulations with explicit solvent, *J. Chem. Theory Comput.*, 2006, **2**, 630.

99 J. G. Ibarra-Armenta, A. Martin-Molina and M. Quesada-Perez, Testing a modified model of the Poisson-Boltzmann theory that includes ion size effects through Monte Carlo simulations, *Phys. Chem. Chem. Phys.*, 2009, **11**, 309.

100 A. Martin-Molina, J. G. Ibarra-Armenta, E. Gonzalez-Tovar, R. Hidalgo-Alvarez and M. Quesada-Perez, Monte Carlo simulations of the electrical double layer forces in the presence of divalent electrolyte solutions: effect of the ion size, *Soft Matter*, 2011, **7**, 1441.

101 G. Luque-Caballero, A. Martin-Molina and M. Quesada-Perez, Polyelectrolyte adsorption onto like-charged surfaces mediated by trivalent counterions: a Monte Carlo simulation study, *J. Chem. Phys.*, 2014, **140**, 174701.

102 F. Oosawa, *Polyelectrolytes*, Marcel Dekker, New York, 1971.

103 H. Schiessel, Charged rosettes at high and low ionic strengths, *Macromolecules*, 2003, **36**, 3424.

104 A. G. Cherstvy, Collapse of highly charged polyelectrolytes triggered by attractive dipole-dipole and correlation-induced electrostatic interactions, *J. Phys. Chem. B*, 2010, **114**, 5241.

105 A. M. Tom, S. Vemparala, R. Rajesh and N. V. Brilliantov, Mechanism of chain collapse of strongly charged polyelectrolytes, *Phys. Rev. Lett.*, 2016, **117**, 147801.

106 J. Bohrisch, C. D. Eisenbach, W. Jäger, H. Mori, A. H. Müller, M. Rehahn, C. Schaller, S. Traser and P. Wittmeyer, *Polyelectrolytes with Defined Molecular Architecture I*, Springer, 2004, pp. 1–42.

107 Y. Levin, Electrostatic correlations: from plasma to biology, *Rep. Prog. Phys.*, 2002, **65**, 1577.

108 D. Andelman, Soft Condensed Matter Physics in Molecular and Cell Biology, Scottish Graduate Series, in *Introduction to electrostatics in soft and biological matter*, ed. W. C. K. Poon and D. Andelman, Boca Raton, Taylor and Francis, 2006, ch. 6, pp. 97–122.

109 A. V. Dobrynin, A. Deshkovski and M. Rubinstein, Adsorption of polyelectrolytes at an oppositely charged surface, *Phys. Rev. Lett.*, 2000, **84**, 3101.

110 A. V. Dobrynin, A. Deshkovski and M. Rubinstein, Adsorption of polyelectrolytes at oppositely charged surfaces, *Macromolecules*, 2001, **34**, 3421.

111 V. Shubin and P. Linse, Effect of electrolytes on adsorption of cationic polyacrylamide on silica: ellipsometric study and theoretical modeling, *J. Phys. Chem.*, 1995, **99**, 1285.

112 N. M. Toan, B.-Y. Ha and D. Thirumalai, in *Polyelectrolyte and polyampholyte effects in synthetic and biological macromolecules*, ed. A. Ciferri and A. Perico,John Wiley & Sons, 2012, ch. 4.

113 A. V. Dobrynin, Electrostatic persistence length of semiflexible and flexible polyelectrolytes, *Macromolecules*, 2005, **38**, 9304, and references cited therein.

114 P. G. Dommersnes, Y. Kantor and M. Kardar, Knots in charged polymers, *Phys. Rev. E: Stat., Nonlinear, Soft Matter Phys.*, 2002, **66**, 031802.

115 M. Ullner, *et al.*, The electrostatic persistence length calculated from Monte Carlo, variational and perturbation methods, *J. Chem. Phys.*, 1997, **107**, 1279, and references cited therein.

116 V. Shubin, Adsorption of cationic polyacrylamide onto monodisperse colloidal silica from aqueous electrolyte solutions, *J. Colloid Interface Sci.*, 1997, **191**, 372.

117 S. Ulrich, A. Laguecir and S. Stoll, Complexation of a weak polyelectrolyte with a charged nanoparticle. Solution properties and polyelectrolyte stiffness influences, *Macromolecules*, 2005, **38**, 8939.

118 M. Seijo, M. Pohl, S. Ulrich and S. Stoll, Dielectric discontinuity effects on the adsorption of a linear polyelectrolyte at the surface of a neutral nanoparticle, *J. Chem. Phys.*, 2009, **131**, 174704.

119 S. Sennato, L. Carlini, D. Truzzolillo and F. Bordi, Salt-induced reentrant stability of polyion-decorated particles with tunable surface charge density, *Biointerfaces*, 2016, **137**, 109.

120 We vary the surface charge density in a very broad range, but still use the solutions of the linear Poisson–Boltzmann equation to compute the PA–surface ES interactions. This is a rather crude approximation: for the potentials well above ≈ 25 mV the non-linear Poisson–Boltzmann theory should be used.[77] In addition to the modified potential distribution profile, the condensation of counterions[97] will set in onto highly charged surfaces, as well as the ordering of water molecules (the Stern layer, in addition to the Gouy–Chapman diffuse layer). This, in turn, reduces the bare surface charge density down to a point when no counterions are getting condensed anymore and thus the overall potential values are not too high any longer for the linear Poisson–Boltzmann theory to be applied. An appropriate consideration of all these additional effects can, however, only be performed in computer simulations with *explicit* ions and solvent molecules.[98–101] The implications of these

(electrochemical) effects on PA–surface adsorption can be the subject of future research, but it requires much larger computer facilities and longer simulation times than used in the current study. The reader is also referred to Section 2.2 of ref. 77 where the description is provided for the charge densities of some highly charged surfaces, such as mica, silica, cement paste, DNA, and some proteins. The values of $|\sigma| \sim 0.1$–0.5 C m^{-2} are not so uncommon in these physical and biological systems—these are also roughly the highest $|\sigma|$ values we use in simulations.

121 For PE–surface adsorption the polymer amount Γ can increase with salt concentration in some range of n_0. The reason is that—despite the polymer–surface ES attraction getting screened more strongly upon the addition of salt—the ES repulsion between the segments of already adsorbed PE chains can be weakened at larger κ, and this effect can be even stronger.[96] Then, higher salt concentrations in the solution n_0 provide a better compaction of PEs on the interface and larger adsorbed amounts, Γ.[31,116] Note also that at very high salinities, with $n_0 \gtrsim 1$ M of simple salt, the amount of PE adsorbed onto the oppositely charged surface often drops rapidly, see ref. 116, so that the maximum of $\Gamma(\kappa)$ dependence at intermediate salt amounts can emerge.[111].